JOURNAL OF GEOPHYSICAL RESEARCH, VOL. 113, E12S35, doi:10.1029/2008JE003097, 2008

Characterization of traverse slippage experienced by Spirit rover on Husband Hill at Gusev crater

Rongxing Li,[1] Bo Wu,[1] Kaichang Di,[1] Anelia Angelova,[2] Raymond E. Arvidson,[3] I-Chieh Lee,[1] Mark Maimone,[4] Larry H. Matthies,[4] Lutz Richer,[5] Robert Sullivan,[6] Michael H. Sims,[7] Rebecca Greenberger,[3] and Steven W. Squyres[6]

Received 31 January 2008; revised 27 May 2008; accepted 22 July 2008; published 8 November 2008.

[1] Spirit rover experienced significant slips traversing Husband Hill. This paper analyzes the slippage Spirit experienced from Sol 154 to Sol 737. Slippage with respect to terrain type and slope is computed using data downlinked from the rover, rover position, and orientation estimations from visual odometry (VO) and photogrammetry based bundle adjustment (BA) method. Accumulated slippage reached a maximum of 83.86 m on Sol 648. However, as Spirit descended into the Inner Basin, the direction of slippage reversed, and accumulated slippage approached zero by the end of the entire traverse. Eight local regions with significant slips and nineteen traverse segments have been analyzed. Slippage was found to be highly correlated to slope direction and magnitude; the reverse of slope directions in the ascending and descending portions of the traverse proves to be the main contributor to the observed cancellation of slippage. While the horizontal component of the slippage almost canceled out, the difference in elevation continually accumulated, mainly during the ascent. In general, long traverse segments created more slips than short ones. This is reflected in both the accumulated and individual slippages. In considering the four major Mars terrain types, Spirit performed best on bedrock, managing to drive on slopes close to 30°. Fine-grain surfaces were the most challenging; though progress was made on slopes up to 15°, slippages of over 100% (more slippage than distance traveled) occurred for short segments. The results of this work can be incorporate into a traverse planning framework in which rover slippage is minimized. Results can be employed in landed planetary missions for precision navigation to avoid potentially dangerous regions by considering expected slippage.

Citation: Li, R., et al. (2008), Characterization of traverse slippage experienced by Spirit rover on Husband Hill at Gusev crater, *J. Geophys. Res.*, *113*, E12S35, doi:10.1029/2008JE003097.

1. Introduction

[2] For both Mars Exploration Rover (MER) mission rovers, Spirit and Opportunity, knowing the exact location of the rover relative to terrain features and targets is of paramount importance for accurate traversing to given locations, especially when approaching specific features and targets with the intent to conduct detailed remote sensing and in situ observations. One technique for localization, wheel odometry, is to track wheel turns and orientation information to determine traverse paths relative to the starting position. This works reasonably well on flat terrains with certain types of surface materials where no wheel slip is encountered. It fails when there is wheel slip, particularly for soil-covered terrains that have significant slopes. Since Sol 154, Spirit traversed rough, soil-covered terrains in Columbia Hills, where traversing flat surfaces is the exception rather than the rule. Thus additional tools are needed to ensure that traverses proceed according to plan. Two new techniques have been employed to achieve higher rover localization accuracy for Spirit, even traversing on the challenging terrains. Visual odometry (VO) [*Matthies*, 1989; *Olson et al.*, 2003; *Maimone et al.*, 2007] computes an estimate of the rover's actual position through tracking image features appearing in sequential images and has been proven to be an effective tool for securing drives on difficult terrain and precision approach to science targets within a relatively short distance. Incremental bundle adjustment (BA) [*Li et al.*, 2002, 2004, 2007] is another technique for rover localization. It provides accurate rover positions

[1]Mapping and GIS Laboratory, Department of Civil and Environmental Engineering and Geodetic Science, Ohio State University, Columbus, Ohio, USA.
[2]Department of Computer Science, California Institute of Technology, Pasadena, California, USA.
[3]Department of Earth and Planetary Sciences, Washington University, St. Louis, Missouri, USA.
[4]Jet Propulsion Laboratory, California Institute of Technology, Pasadena, California, USA.
[5]DLR Institute of Space Simulation, Cologne, Germany.
[6]Department of Astronomy, Cornell University, Ithaca, New York, USA.
[7]NASA Ames Research Center, Moffett Field, California, USA.

0148-0227/08/2008JE003097$09.00

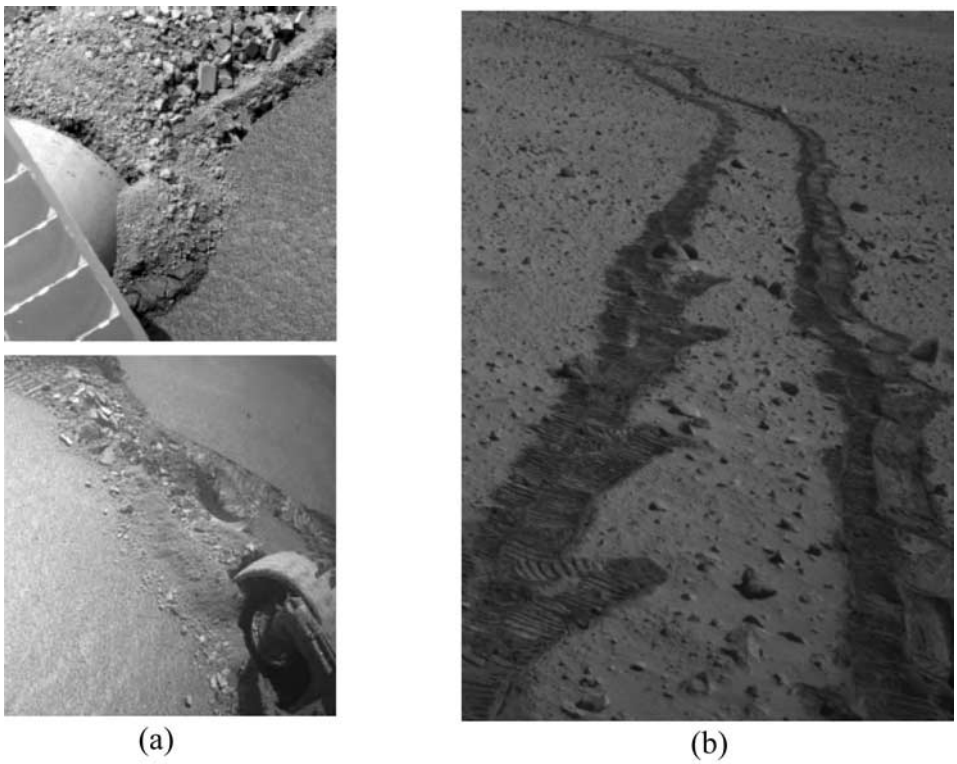

Figure 1. Rover slippage: (a) wheel of Opportunity rover trapped in the Purgatory dune on Sol 447 (top) and view of gouged track after rover finally escaped (bottom) and (b) downslope view of rover track showing extensive slippage as Spirit climbed an upslope close to West Spur on Sol 325.

by building a strong image network along the traverse to maintain consistent overall traverse information. The combined localization results allow one to precisely link together the various segments of traverses and are important both for understanding where the rover is with respect to potential obstacles or targets of interest and for adjusting the planned path with consideration of rover slips, as well as for referencing to the global Mars body-fixed frame, thus allowing placement of the traverses onto orbital data sets such as those provided by Mars Orbiter Camera (MOC), Context Camera (CTX), Compact Reconnaissance Imaging Spectrometer for Mars (CRISM), and High Resolution Imaging Science Experiment (HiRISE) images.

[3] Both Spirit and Opportunity rovers have the same hardware configurations and carry the same Athena science payload [*Squyres et al.*, 2003]. The rovers are six-wheeled, solar-powered robots that measure 1.5 m high, 2.3 m wide and 1.6 m long. They weigh 180 kg, 35 kg of which is the wheel and suspension system. Each wheel is approximately 26 cm in diameter, and both the front and back wheels are steerable. Both rovers experienced significant slippages during their explorations of the Martian surface. Opportunity experienced an accumulated slippage of 18.71 m over a distance of 91.42 m (20.5%) for over 60 Sols within Eagle Crater where the spacecraft landed [*Li et al.*, 2007]. This slippage was caused mainly by the crater's loose soils and the steep slopes of the crater wall. Figure 1a shows an extreme case where the trapped wheel and slip track were imaged when Opportunity rover was trapped in the Purgatory dune on Sol 447. The top image in Figure 1a shows how the right rear wheel of the rover was almost covered by sand. The rover experienced a continuous slip motion here as the wheels continuously rotated without any actual movement of the vehicle. The bottom image in Figure 1a shows the trench created by the rover wheel that was revealed after the rover successfully maneuvered out of the dune. Spirit rover's accumulated slippage was as large as 56.61 m over a distance of 543.77 m (10.4%) in the Husband Hill area [*Li et al.*, 2006]. Figure 1b shows wheel tracks exhibiting example wheel slips experienced as Spirit climbed upslope on Sol 325.

[4] Figure 2 illustrates the significant slippage Spirit experienced as the rover traveled across Husband Hill from Sol 154 to Sol 737. The blue line in Figure 2 shows the rover traverse at Husband Hill computed from wheel odometry data with some short segments of VO corrections. In contrast, the red line is the optimal traverse estimated by BA. Details about the methods employed for obtaining these two lines are given by *Li et al.* [2005]. Before Spirit arrived at the foot of Husband Hill on Sol 154, its accumulated slippage was 26.53 m over a distance of 3 km (0.9%) from the lander. Starting from Sol 154, when Spirit began ascending Husband Hill and we reset the accumulated distance as zero for this study, its accumulated slippage increased. When the rover reached the summit on Sol 648, the accumulated slippage had reached a maximum of 83.86 m over a distance of 1.5 km (5.3%). However, when Spirit descended to Inner Basin (Sol 710) and then further downhill on the way to Home Plate (Sol 737), the accumulated slippage decreased to 6.13 m over a distance of 2.6 km

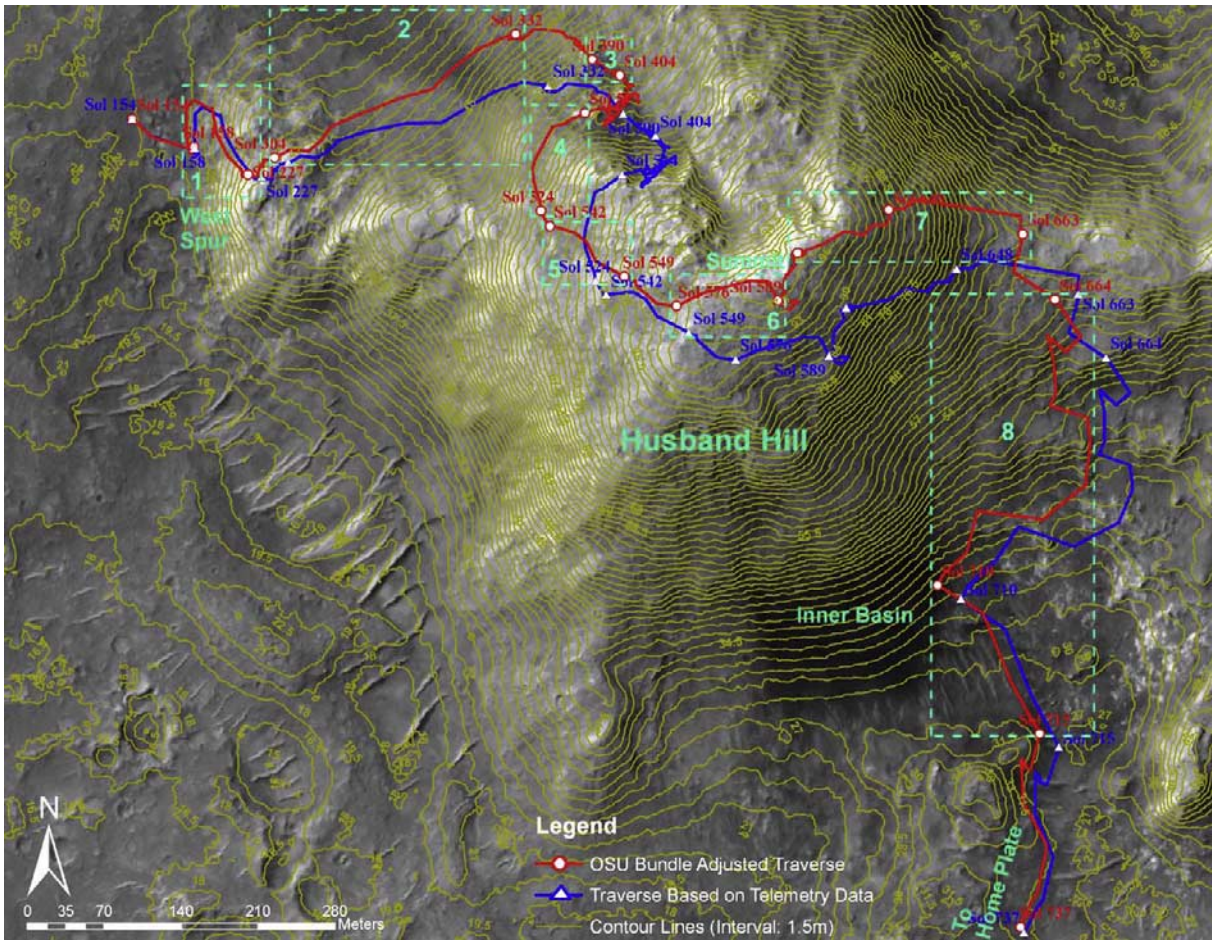

Figure 2. Spirit traversed Husband Hill for Sols 154 to 737. The blue line illustrates the traverse computed from telemetry. Red presents the traverse with corrections by bundle adjustment (BA). The background map is based on High Resolution Imaging Science Experiment (HiRISE) image [*McEwen et al.*, 2007], and contour lines are derived from the stereo HiRISE images by U.S. Geological Survey [*Kirk et al.*, 2007]. Local regions of major slippage are framed and numbered 1–8 in light blue color.

(0.2%). The slip as discussed in this paper is associated with terrain types and slopes and therefore, the level of the slip varies along the traverse as these factors changes. From Sol 154 to Sol 737, after traversing uphill and downhill for 2.6 km, the accumulated slippage experienced by Spirit seemed to have been canceled out. However, the difference in elevation over the same period increased regardless of the trend of the traverse slips (Figure 3). This paper presents the effort and results of characterization and analysis of the Spirit rover slippage occurring during the drive at Husband Hill.

2. Previous Research on Mars Rover Slip

[5] Early studies on vehicle slip using Mars data were conducted for Viking and Mars Pathfinder (MPF) missions [*Moore et al.*, 1977, 1999]. This analysis consisted of a controlled, one-wheel experiment in which soil parameters can be inferred by measuring the occurred slip. Similar experiments have been performed in the MER mission [*Arvidson et al.*, 2004]. A related analysis has also been done for inferring the soil parameters by observing cleat marks and measuring their depth from stereo imagery [*Richter et al.*, 2005]. Further research on wheel slippage of mobile robots and planetary rovers focused on three issues: physical and geometrical properties of the terrain [*Perko et al.*, 2006], rover mechanism [*Michaud et al.*, 2006; *Reina et al.*, 2006], and rover-terrain interaction [*Richter et al.*, 2006; *Helmick et al.*, 2005, 2007; *Angelova et al.*, 2006, 2007]. *Perko et al.* [2006] conducted a soil mechanics investigation wherein soil mechanical properties were determined by computer reconstruction of mass wasting features observed in photographs of MER landing sites, and the natural slope stability was analyzed by characterizing the shear strength, grain-size distribution, and densities of various Mars soil simulants with standard laboratory measurements. The ability of a given simulant to appropriately represent the mechanical properties of in situ Mars soils was judged, and specific simulants were recommended for certain regions of Mars to help estimate the possible rover slippages. *Michaud et al.* [2006] investigated rover stability and ability for slope and obstacle climbing from a wheel design optimization point of view. *Reina et al.* [2006] described methods for wheel slippage and sinkage detection taking into consideration physical characteristics of the vehicle and its environment. *Richter et al.* [2006] presented

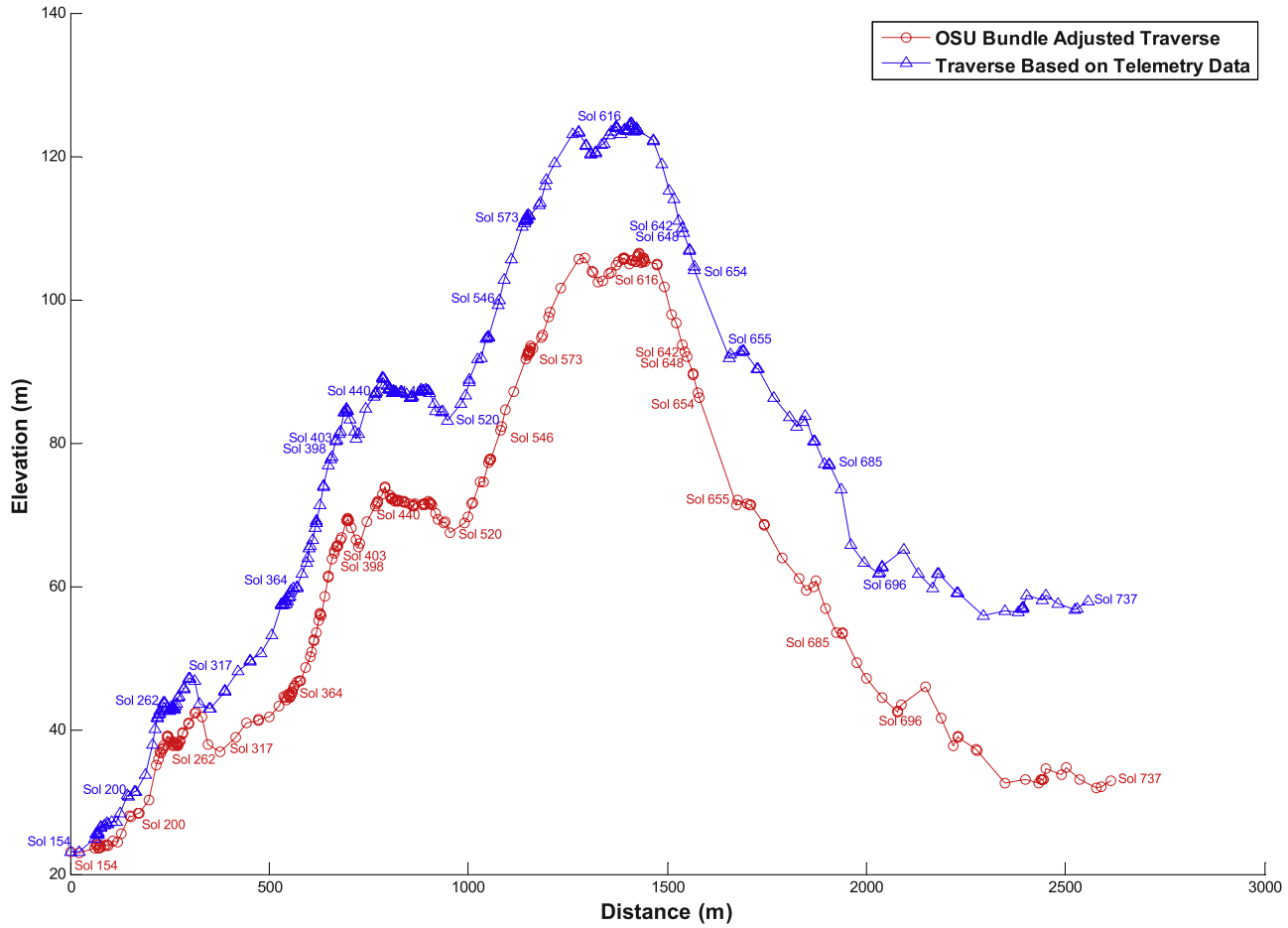

Figure 3. Vertical profiles of BA-computed (red line) and telemetry-based (blue line) Spirit traverses of Husband Hill for Sols 154 to 737. Note: The scales of the horizontal and vertical axes are different.

a tractive prediction module that handles the wheel-terrain interaction, from which the estimation of the rover chassis motion performance on a particular soil can be achieved. *Angelova et al.* [2006] focused on prediction of slip from a distance for wheeled ground robots using visual information as input. The predicted slip is intended to be used for better path planning and avoiding of areas where the rover may be trapped because of slippage. Experiments from several off-road terrains (including soil, sand, gravel, and woodchips) demonstrated that the slip prediction error is about 20% of the step size [*Angelova et al.*, 2006, 2007].

[6] Onboard wheel odometry, Inertial Measurement Unit (IMU), and Sun-finding techniques were primarily used for rover localization in the MER mission. When the rover travels, for example, on slopes or loose soils, significant slips may be experienced and ground operations can be affected. Visual odometry (VO) can estimate the actual rover position and attitude by tracking features in consecutive Navcam stereo images taken at short steps (e.g., every 25 cm). These estimates can be used to correct the kinematics position obtained from wheel odometry. From the stereo images, dozens of terrain features are autonomously located and tracked, resulting in dozens of motion vectors that are robustly filtered to produce an accurate measurement of overall vehicle motion [*Olson et al.*, 2003; *Cheng et al.*, 2006; *Maimone et al.*, 2007]. Telemetry data in this paper refers to data downlinked from the rover including position and orientation information derived from on board observations of wheel odometry, IMU, and Sun-finding images. Whenever VO is performed, such corrected position and orientation information (on board) is also included in the telemetry data downlinked from the rover. The bundle adjustment (BA) technology uses all available images taken by Navcam and Pancam at relatively longer steps (e.g., a few meters to 30 m) and the telemetry data as input to build an image network. The pointing parameters (camera center position and three rotation angles) of each image in the network are adjusted to their optimal values as determined by the least squares method. In this way, the rover's position at the time taking images can be computed and, highly accurate localization of the rover along the traverse can be achieved [*Li et al.*, 2006, 2007]. VO and BA have been combined and applied to correct wheel slippage, azimuthal angle drift and other navigation errors and to provide accurate rover traverse information. While VO was performed onboard the rovers for short distances on large slopes, or when approaching science targets, the BA computation was conducted on Earth for the overall traverse. Table 1 summarizes different equipment and methods used for rover localization and slippage computation.

[7] In this paper, we focus on characterization and analysis of rover slippage based on actual data collected when

Table 1. A List of Equipment and Methods Used in Rover Localization and Slippage Computation

Equipment or Method	Remark
Wheel odometry	On board, distance and azimuth measurements
IMU	On board, three orientation angles in the Mars body fixed frame
Sun-finding images	On board, azimuth angle measurements using Pancam
Visual odometry	On board, rover position and orientation with short drives using Navcam images
Bundle adjustment	On Earth, rover position and orientation of the entire traverse using Navcam and Pancam images

the Spirit rover traversed up and down Husband Hill, covering more than 2.6 km over several different soil types and slopes. Rover slips are recognized as one of the key limiting factors for rover localization, navigation, and many other rover activities in the current MER mission [*Leger et al.*, 2005; *Biesiadecki et al.*, 2006]. This analysis can be used to provide new insights into the soil types available on Mars and new understanding of rover mobility and interaction with the terrain. Being able to accurately characterize this slippage will have significant impact on the ongoing MER and future Mars rover missions by enabling more intelligent path planning, predicting the expected slip, and preventing the rover from being trapped.

3. Spirit Rover Traverse and Slip at Husband Hill

[8] After traversing 3 km, Spirit rover reached Husband Hill on Sol 154 (Figure 2). Husband Hill rises to a height of 83.6 m above the plain just to the west of the West Spur, or 106 m above the lander. It also has the most challenging terrain the rover has had to traverse. The rocks composing Husband Hill are crustal sections formed by volcaniclastic processes and/or impact ejecta emplacement [*Arvidson et al.*, 2006]. To traverse it, Spirit had to drive on steep slopes (10 to 30°) while constantly maneuvering around hazardous rocks and drop offs and dodging sandy patches where the rover could slip or dig in and get stuck.

[9] The rover positions derived from telemetry represent the initial positions (blue line in Figures 2 and 3). As already mentioned, the initial positions from telemetry are not precise because they are affected by rover slips. We compare them with better determined positions provided by BA for this traverse in Figure 2. BA corrections are performed on Earth and presented by the red line. Thus the differences between the initial positions from the telemetry data and those from BA can be used to estimate rover slippage.

[10] At Husband Hill, Pancam and Navcam images were obtained at many different locations. The Pancam images were acquired mainly at locations where substantial science investigations took place, while the Navcam images were taken more frequently for navigation and near-rover site characterization. Using all these images, BA of the image network was performed incrementally at each rover location by fixing the previously adjusted image positions and orientations and adjusting the newly acquired images at the new locations [*Li et al.*, 2004]. To track the positions and analyze positioning errors, the traverses are derived in the landing site cartographic (LSC) coordinate system, which is an east-north-up (x-y-z) and right-handed local coordinate system with its origin at the lander's position [*Li et al.*, 2006]. Starting from Sol 154 the locally accumulated difference between these two traverses increases as Spirit climbed the northwest facing slope of Husband Hill. On Sol 648 the rover reached the maximum difference of 83.86 m around the summit (or 5.3% of the 1.5 km traveled from Sol 154), and decreased afterward as Spirit traveled downhill on south facing slopes. At the end of this traverse (Sol 737), the planemetric and 3D accumulated differences were 6.13 m and 25.61 m, respectively, or 0.23% and 0.98% of the total distance of 2.6 km traveled. This means that the differences between the rover locations from telemetry and those after BA almost canceled each other out in the Husband Hill area. Figure 3 illustrates the vertical profiles of the telemetry- and BA-derived traverses from Sols 154 to 737. It shows that whether the rover drives uphill or downhill, the telemetry-derived elevation is always higher than that estimated by BA.

[11] Localization errors in the telemetry data were mainly caused by wheel slip. Particularly, the rover slip exhibited significantly different behavior when Spirit encountered upslope and downslope terrain in the Husband Hill area. In sections 4 and 5, we characterize the rover slippage in detail by using geometry and attribute data collected at Husband Hill, and analyzing factors causing rover slippage, as well as the relationships between the factors.

4. Description of Rover Slippage, Collected Data, and Primary Analysis

4.1. Definition of Rover Slippage

[12] Rover slippage is considered to be a measure of the lack of progress or the lack of mobility of the rover on a certain terrain [*Helmick et al.*, 2004; *Angelova et al.*, 2006]. When VO is used to provide the better estimated positions at each step (e.g., 5–50 cm) the rover's position and attitude is calculated [*Helmick et al.*, 2004, *Angelova et al.*, 2006]. VO is shown to be an accurate method for vehicle motion estimation [*Olson et al.*, 2003; *Helmick et al.*, 2004] and has proved to be a critical tool for correct localization for both MER rovers in areas of large slip [*Maimone et al.*, 2007]. However, in the MER mission, obtaining VO supported rover positions at each step of the rover is impossible because longer distance drives (usually consisting of autonomous or blind drives) would have been significantly slowed down because of high computational costs. Therefore, VO has been run onboard Spirit rover wherever necessary.

[13] BA images have been taken regularly wherever Spirit stopped, and BA computation has been performed on Earth [*Li et al.*, 2004]. For the BA-estimated positions, the traverse segments are much longer than VO segments, ranging from 0.01 m to 96.78 m, with an average of 8.58 m. The traverse segment is defined as the interval between two consecutive BA positions where the rover stops. In this paper, the BA positions are used as the better estimated positions of the actual positions, while the positions derived from telemetry data are considered as positions where slip may exists. Slippage is determined by the difference between these two derived positions.

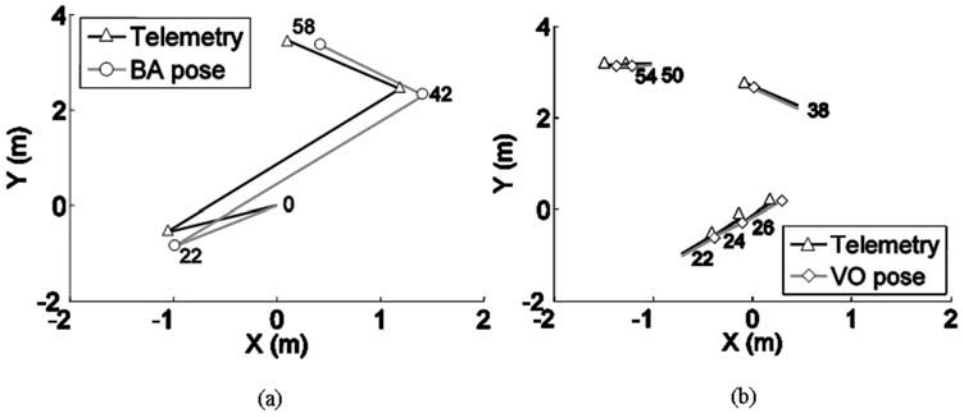

Figure 4. Slip measurements from BA and visual odometry (VO). (a) BA segments at Site 85 (Sols 222–227) and (b) corresponding VO steps. Rover Motion Counter (RMC) numbers are marked to identify the segments and steps.

[14] In the case of VO, a single step (corresponding to a motion command) of the rover is relatively small and therefore a much more precise estimate of the actual position can be obtained [*Maimone et al.*, 2007]. However, VO-based slip measurements are not available at each step of the rover. Figure 4 shows a special situation where both VO and BA were performed at Site 85 of Spirit rover. BA positions are computed at four locations where the rover made full stops with rover motion counter (RMC) numbers 0, 22, 42 and 58 (Figure 4a). But VO was only performed for selected steps in between, starting at RMC numbers 22, 24, 26, 38, 50 and 54 (Figure 4b). Obviously, BA segments are only partially covered by VO steps in this case.

[15] The significant advantage of BA estimates is that they can be computed over longer distances and throughout the entire traverse to give precise rover positions. This is complemented by the advantage of VO that it provides a more reliable and accurate estimate of slip at small steps.

[16] The following notations are used in the analysis of rover slippage (Figure 5):

[17] Accumulated slippage S: Difference of the traverse end positions of BA and telemetry traverses.

[18] Individual slippage ΔS_i: Difference between the two ith traverse segments from BA and telemetry traverses.

[19] Longitudinal slippage ΔS_{long}: the longitudinal component of individual slippage ΔS along the rover's drive direction (Figure 5b).

[20] Lateral slippage ΔS_{lat}: the lateral component of individual slippage ΔS perpendicular to the rover's drive direction (Figure 5b).

[21] Longitudinal slope D_{long}: the slope along the rover's drive direction (Figure 5c), which corresponds to longitudinal slippage.

[22] Lateral slope D_{lat}: the slope perpendicular to the rover's drive direction (Figure 5c), which corresponds to lateral slippage.

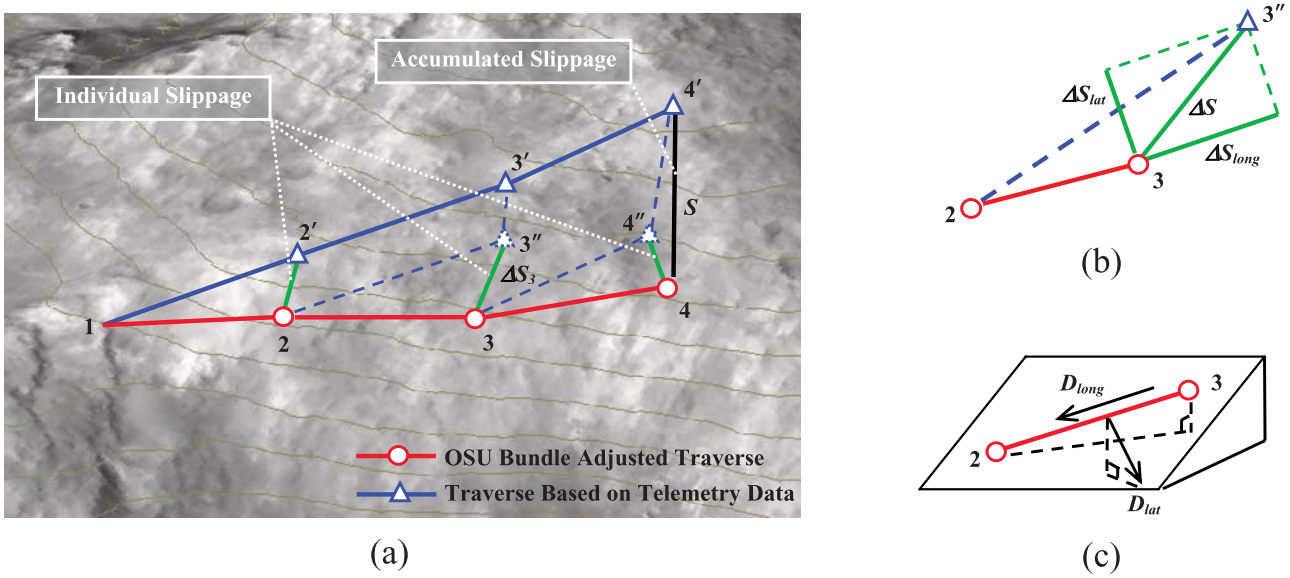

Figure 5. Rover slippage: (a) illustration of upslope slip from traverse points 2, 3, and 4 (BA locations) to 2′, 3′, and 4′ (telemetry locations), (b) two components of the individual slippage ΔS: ΔS_{long} and ΔS_{lat}, and (c) two components of terrain slopes: D_{long} and D_{lat}.

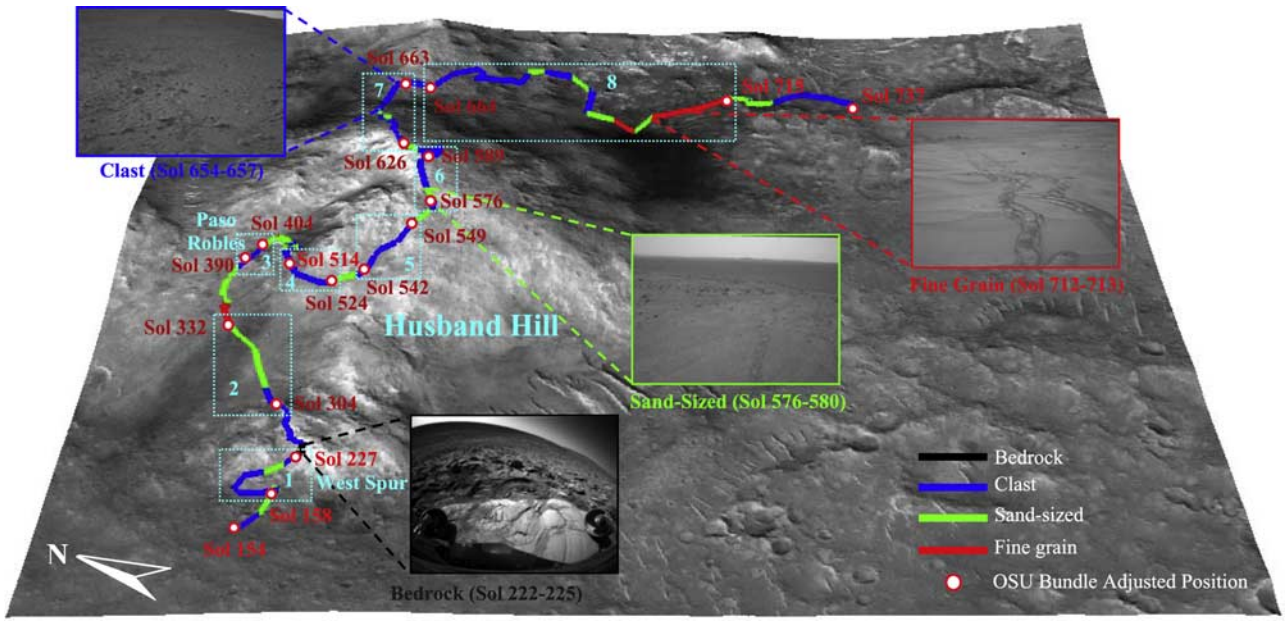

Figure 6. The traverse segments at Husband Hill are classified into bedrock (black), clast (blue), sand-sized (green), and fine grain (red). Local regions of major slippage (numbered 1–8 in light blue).

[23] When describing slippage for a short traverse created, for example, when the rover approaches a specific target, the absolute value of the individual slippage is an adequate measure. For a long traverse, however, rover slippage is better measured as a percentage of the traverse length. For this purpose, individual slippage, ΔS, and its two components, ΔS_{long} and ΔS_{lat}, can be normalized (divided) by the length of the corresponding traverse segment. They are then expressed as $\overline{\Delta S}$, $\overline{\Delta S}_{long}$, and $\overline{\Delta S}_{lat}$, respectively.

[24] Longitudinal slippage often occurs on soft terrain, with significant and generally obvious effect; the rover traverse is squeezed or stretched in the direction of movement. Lateral slippage often occurs on relatively hard terrain with a slope and is not always significant. Accumulated lateral slippage causes the rover to deviate from its direction of movement.

4.2. Terrain Classification

[25] Terrain classification is based on visual interpretation of the available rover traverse images. These images include Pancam and Navcam images. Hazcam images, which are front and rear looking and are usually taken at the ends of traverse segments, are also used. Martian terrain has been categorized into different categories, for example, drift, crusty-to-cloddy, blocky, and rocks [*Moore et al.*, 1977]. It was further classified as drift, cloddy, indurated, and rocks [*Moore et al.*, 1999]. *Leger et al.* [2005] used windblown sand, regolith, encrusted soil, and bedrock. After carefully observing the collected Pancam, Navcam and Hazcam images at Husband Hill in our analysis, we classified the terrain for each traverse segment using four general categories: bedrock, clast, sand-sized, and fine grain (see Figure 6 for representative examples). In contrast to terrain categorizations by *Moore et al.* [1977, 1999] and *Leger et al.* [2005], this terrain classification scheme was developed from the point of view of expected rover mobility rather than soil parameters. For example, we have added clast as a terrain type because it causes a different level of rover slip compared to homogeneous soils or rocks. It should be noted, however, that this terrain classification assigned only an average or dominant terrain type for each traverse segment, which may be short or long and may contain different terrain types. This may cause terrain classification errors for a long segment that does not have a homogeneous terrain type. Figure 6 illustrates the terrain classification for all the traverse segments in the study area.

4.3. Terrain Slopes

[26] As pitch and roll angles of the rover are associated with slippage for a fixed terrain type [*Bekker*, 1969; *Terzaghi*, 1996; *Angelova et al.*, 2006], we decompose the terrain slope of a traverse segment into longitudinal (along the direction of forward motion) and lateral (perpendicular to the direction of forward motion) components D_{long} and D_{lat} (Figure 5c). The longitudinal slope of a traverse segment can be calculated from bundle-adjusted elevations of segment end positions. An upslope segment produces a positive longitudinal slope, and a downslope segment a negative longitudinal slope. For the lateral slope calculation, a local digital elevation model (DEM) is employed. First, the maximum slope of a segment is obtained by comparing slopes in eight different directions. Each of the eight slopes is computed by linear fitting a corresponding elevation profile, which is derived from the DEM in a direction and centered on the midpoint of the segment. Then, the maximum slope is projected in the lateral direction and is used as the lateral slope. The DEM uses two products, one (grid spacing 50 cm) covering the summit area of Husband Hill and generated by the OSU Mapping and GIS Laboratory using Pancam and Navcam images, the other (grid spacing 1 m) covering the rest of the area and generated by USGS using

Table 2. Traverse Data Summary

Traverse Distance Derived From BA/Number of Segments[a]	Traverse Segment			Terrain Type										Terrain Slope (°)							
	Length, L (m)			Bedrock			Clast			Sand-sized			Fine grain			Downslope			Upslope		
	Max	Min	Mean	Number of Segments	Distance Traversed (m)	Percentage	Number of Segments	Distance Traversed (m)	Percentage	Number of Segments	Distance Traversed (m)	Percentage	Number of Segments	Distance Traversed (m)	Percentage	Longitudinal (D_{long})	Lateral (D_{lat})		Longitudinal (D_{long})		Lateral (D_{lat})	
																Max	Mean	Max	Mean	Max	Mean
2616 m/305	96.78	0.01	8.58	7	25.89	0.99	157	1503.07	57.46	111	847.25	32.39	30	239.85	9.17	33.85	6.10	19.04	5.50	18.36	7.16	20.22	6.07

[a]BA is bundle adjustment.

HiRISE orbital images [*Kirk et al.*, 2007]. For the convenience of later analysis, we ignored the orientation of the lateral slope and only considered its absolute magnitude.

[27] It should be noted that the longitudinal and lateral slopes are derived from DEM or stereo image measurements. However, in VO computation, there is an additional mechanism for rover attitude estimation from IMU data (Table 1) because the local attitude angles of pitch, roll and yaw can be computed from the three global IMU angles in the Mars body fixed frame. Since slippage analysis based on VO data covers shorter distances, pitch and roll angles from the IMU are employed as the longitudinal and lateral slopes of the terrain.

4.4. Traverse Segment Data and Derived Summaries

[28] For further rover slippage analysis, data derived from both BA (that covers the entire period when Spirit ascended and descended Husband Hill) and from VO (that covers only a small portion of the traverse) were collected. The bundle adjusted rover traverse has 305 segments, covering a traverse distance of 2616 m. The minimum elevation is 22.87 m (Sol 154) and the maximum 106.47 m (Sol 623), making a maximum elevation difference of 83.6 m in the Husband Hill area. Table 2 summarizes the data set of the traverse segments used for BA.

[29] The VO position and orientation estimates and the rover tilt measurements obtained in the Husband Hill area are used as a tool for independent slippage analysis of the same traverse considered in the BA data set. Though the VO data could not be obtained for all BA segments, whenever available it provides local and detailed rover slip and terrain slope information within the BA segments. The VO data contains 511 segments in total and covers 222 m. They are unevenly distributed along the traverse. For example, for some sols we have only VO measurements covering partial BA segments, whereas for other sols, when pose estimation was critical or a lot of slip was encountered, we have VO measurements for entire BA segments. Table 3 summarizes the VO data set.

5. Rover Slippage Characterization and Analysis

[30] The data collected for rover slippage analysis at Husband Hill is from multiple sources. Telemetry data contains rover position information derived from onboard sensors including wheel odometry, IMU and Sun-finding images. Corrections by VO are included if performed. Improved rover locations are estimated by BA technology. Terrain classification is performed by interpretation of rover images (Hazcam, Navcam and Pancam) by an operator. Slopes are calculated from DEMs derived from rover images wherever available, or from orbital images, such as HiRISE images. The slippage parameters are computed by comparing the rover positions from VO, BA and telemetry data. The advantages of slippage estimated in this way are high-quality slip information over all traverse segments and ready information for examination of general trends.

5.1. General Trend

[31] On the basis of BA data, along the rover traverse at Husband Hill, the total individual slippage ($\Sigma\Delta S_i$) is 362.29 m. The accumulated slippage (S) reached a

Table 3. Traverse Data Summary

Traverse Distance Derived From VO/Number of Segments[a]	Traverse Segment			Terrain Type										Terrain Slope: Absolute Slope (°)			
	Length, L (m)			Bedrock			Clast			Sand-sized			Fine grain			Longitudinal (D_{long})		Lateral (D_{lat})	
	Max	Min	Mean	Number of Segments	Distance Traversed (m)	Percentage	Number of Segments	Distance Traversed (m)	Percentage	Number of Segments	Distance Traversed (m)	Percentage	Number of Segments	Distance Traversed (m)	Percentage	Max	Mean	Max	Mean
222 m/511	0.72	0.05	0.51	13	3.97	1.78	228	107.80	48.50	218	87.97	39.58	49	16.39	7.37	27.36	10.32	22.98	6.61

[a]VO is visual odometry.

maximum of 83.86 m (around the summit, on Sol 648) and the individual slippage (ΔS) has a maximum of 15.46 m at segment 255 (Sols 654–655). This segment is the longest (96.78 m), when Spirit descended a downslope as large as 15°. Further, the normalized individual slippage ($\overline{\Delta S}$) reached a maximum of 121% at segment 101 (Sols 398–403), where Spirit traveled a short distance of 0.42 m on clast terrain and experienced a slip of 0.51 m at a downslope of 5.86°.

[32] Figure 7 shows accumulated and individual slippages versus traverse segment IDs. The corresponding elevation profile from BA is illustrated as well. The accumulated slippage (S) has a similar general trend as the elevation (z) along the traverse. It increases when the rover climbed uphill and decreases as the rover descended downhill. The individual slippage is plotted in line with crosses. The high occurrences of major individual slippages are separated and numbered in 8 traverse regions, which are also marked by rectangles in Figures 2 and 6. It is very clear that these 8 regions of high individual slip activities correspond to significant changes in the accumulated slippage.

5.1.1. Slippage and Slope Directions

[33] Table 4 lists the details of slippages of these 8 local regions. The length of the traverse in the region D_i varies from 32 m to 629 m. For each region, its total accumulated slippage within the region S_i and their ratio S_i/D_i are given in percentages. Another measure is the ratio between the accumulated slippage within the region S_i and the accumulated slippage of the entire traverse S (362.29 m), which shows the individual contribution of each region toward the overall accumulated slippage. The last column lists the difference Diff. S_i between the first and last accumulated slippages of each region. The following is a brief description of rover activities in the 8 regions.

[34] In Region 1 (Sol 158 to Sol 227), Spirit started to climb toward West Spur (Figure 6). The rover reached the base of West Spur during the fall season for the Martian southern hemisphere, when the Sun was north relative to the latitude of the landing site. Because of the poor solar situation and steady accumulation of dust on the solar panels, the rover usually was commanded to stay on slopes with north facing surface normals in order to maximize sunlight on the solar panels [*Arvidson et al.*, 2006]. The rover first drove northward along the foot of West Spur, and then turned south to ascend the Spur. The rover was kept on north and northwest facing slopes during the ascent, so slippage inside this region is also generally toward the north or northwest (Figure 2) with an accumulated slippage of 11.94 m (Diff. S_1). In Region 2 (Sol 304 to Sol 332), the rover descended the eastern flank of the Spur and drove onto the saddle between West Spur and Husband Hill. Within this local region, the rover traveled mostly on north facing slopes (Figures 2 and 6), so the slippage is also toward the north, and accumulated slippage then increased with an amount of 42.61 m (Diff. S_2). In Region 3 (Sol 390 to Sol 404), the rover was conducting measurements on several rocks and outcrops on the northwest flank of Husband Hill. The major slips in this region happened when the rover was preparing to examine the Paso Robles bright soil deposits (Sol 397 to Sol 398). This further increased the overall accumulated slippage by 6.98 m

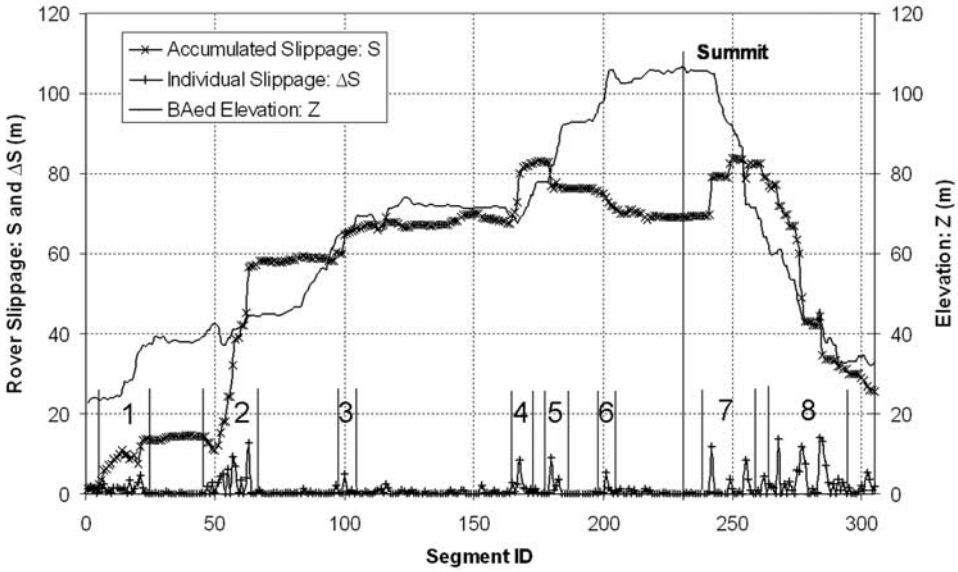

Figure 7. Individual (ΔS) and accumulated (S) rover slippages plotted against elevation of the traversed terrain at Husband Hill. Eight regions illustrated by the vertical bars and IDs from 1 to 8 are identified for significant individual slippages, and their correlation with the accumulated slippage is discussed in the text.

(Diff. S_3). The constraint that the rover must travel on a path with north facing slopes was alleviated in the late winter, between Sol 419 and Sol 420, when wind gusts removed much of the dust that had accumulated on the solar panels and power availability increased. Also, the migration of the Sun southward as the rover conducted operations throughout the winter and into the spring season further alleviated the need to stay on slopes with north facing normals [*Arvidson et al.*, 2006]. Therefore the rover was able to travel southward to climb Husband Hill. In Region 4 (Sol 514 to Sol 524), while Spirit drove south along the valley of Husband Hill, most of its traverse was on northwest facing downslopes (Figure 6). Therefore, rover slippage is mainly toward the northwest, and accumulated slippage still increases within this local region (Figure 2) by 15.04 m. In Region 5 (Sol 542 to Sol 549), the rover ascended Husband Hill quickly along the valley, where the traverse was mainly on southwest facing upslopes (Figure 6), so the rover slippage reverses to southwest slippage and the accumulated slippage then decreases for the first time to a significant level of −6.32 m (Figures 2 and 7). In Region 6 (Sol 576 to Sol 589), the rover drove eastward, approaching the summit of Husband Hill. Most of its traverse was on south facing slopes (Figure 6), so the rover slippage is also mainly toward the south and the accumulated slippage continued to decrease (Figure 7) with a value of −3.91 m. In Region 7 (Sol 626 to Sol 663), the rover continued driving northeast and east along the ridge of Husband Hill. Accumulated slippage began to increase again because of large rover slip events, for example, the significant rover slide on Sol 654 (Figure 3). In Region 8 (Sol 664 to Sol 715), the rover traveled mainly on south facing slopes as Spirit descended Husband Hill (Figure 6). The rover slips were also mainly toward the south, and the accumulated slippage decreased quickly (Figure 7) with a significant value of −47.15 m.

[35] Particularly, the measure of the contribution of the individual slippage in a region toward the total slippage of the traverse (S_i/S in Table 4) explains that the large local individual slips in Regions 2, 7 and 8 have a significant impact on the accumulated slippage S (also see Figure 7). Furthermore, such an impact is slope direction dependent and the overall effect of the slips is much reduced in the Husband Hill area because of the balanced distribution of slope directions.

Table 4. Eight Regions of Major Individual Slippage

Region	Segment ID	Sol	D_i (Traverse Length in Region i)	S_i (Accumulated Slip in Region i)	S_i/D_i (%)	S_i/S (%)	Difference S_i
1	4 ∼ 24	158 ∼ 227	158.46 m	29.21 m	18.43%	8.06%	11.94
2	46 ∼ 64	304 ∼ 332	258.04 m	61.15 m	23.70%	16.88%	42.61
3	96 ∼ 102	390 ∼ 404	31.67 m	8.72 m	27.53%	2.41%	6.98
4	164 ∼ 172	514 ∼ 524	111.54 m	18.73 m	16.80%	5.17%	15.04
5	179 ∼ 185	542∼ 549	90.69 m	15.92 m	17.55%	4.39%	−6.32
6	200 ∼ 205	576 ∼ 589	102.06 m	8.92 m	8.74%	2.46%	−3.91
7	240 ∼ 258	626 ∼ 663	266.67 m	39.98 m	14.99%	11.03%	13.01
8	262 ∼ 292	664 ∼ 715	628.62 m	107.97 m	17.18%	29.80%	−47.15

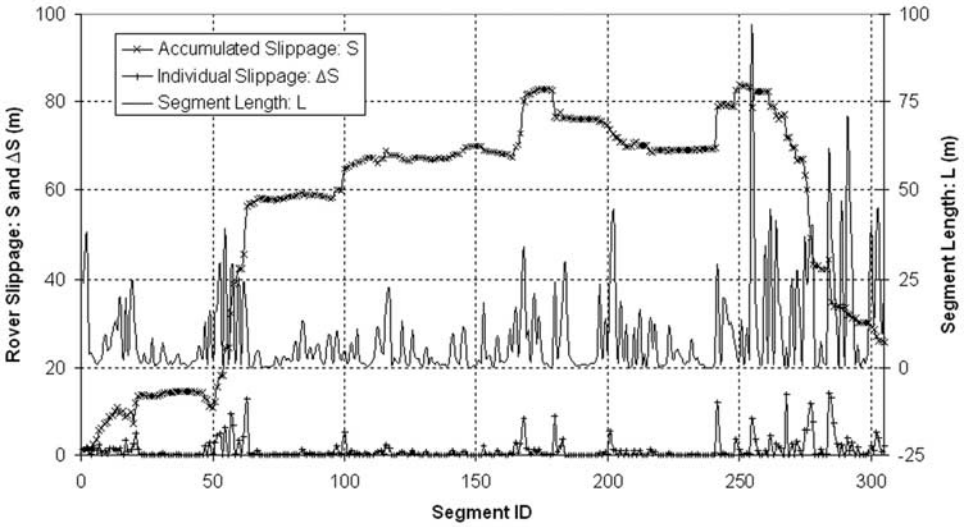

Figure 8. Individual and accumulated rover slippages with respect to traverse segment length.

5.1.2. Slippage and Traverse Segment Length

[36] There are two types of drives on a typical drive sol, blind drive and autonomous drive. The blind drive is usually commanded on the basis of the fact that the path in the immediate front of the rover can be seen very clearly in Navcam or Pancam images and is considered safe. The rover then drives to a point that is often a relatively far point, e.g., 25 m away. This is subsequently followed by an autonomous drive with help of on board navigation software that can detect obstacles and find an updated new optimal route to the target. This type of drive may be short or long depending on the terrain situation, but increases the distance that a rover can drive each sol. On an approach sol, e.g., to reach a specific target with particular science significance (such as a rock, outcrops or soils), a short distance may be driven and VO is often used. Such short drives may not highly contribute to the overall slippage. However, if not corrected their relative slippage can appear larger because of the short traverse segment lengths.

[37] Long traverse segments usually occur on drive sols, when the rover performs a blind drive and often a subsequent autonomous drive over a relatively long distance. BA of the long traverse segments are carried out by using Pancam or Navcam images. The relationship between rover slippage and traverse segment length is illustrated in Figure 8. As can be seen from Figure 8, the accumulated slippage increases or decreases rapidly when the rover drives on long traverse segments. This is especially true as the rover climbed the hill (around segment 60 in Figure 8) and descended rapidly in the last part of the traverse. It can also be noted that large individual slips are also associated with long segments.

5.1.3. Anomalous Traverse Segments

[38] Normalized individual slippage $\overline{\Delta S}$ is an effective measure used to find anomalous traverse segments. Figure 9 shows the normalized individual slippage along the rover traverse at Husband Hill. To identify anomalous segments, a number of segments can be selected for further analysis using a threshold of three times the standard deviation. A

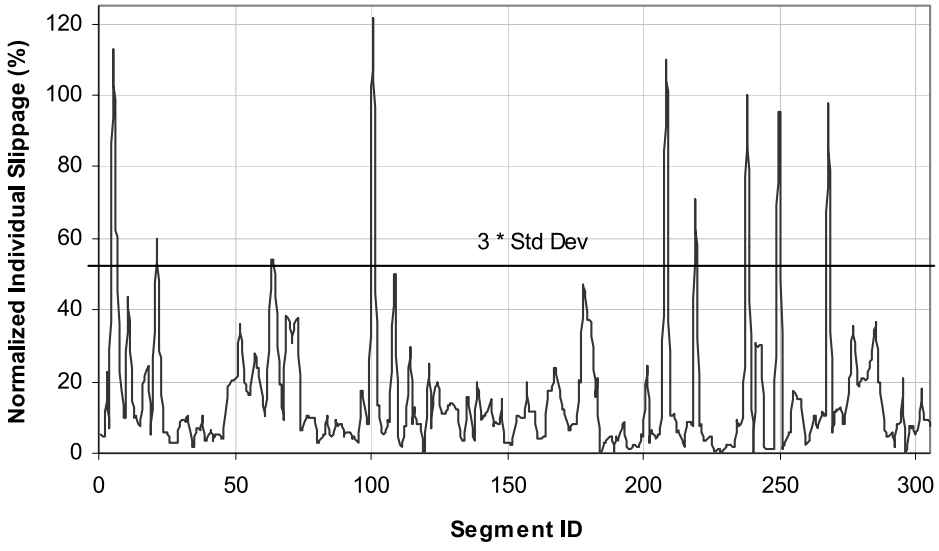

Figure 9. Normalized individual slippage and a threshold.

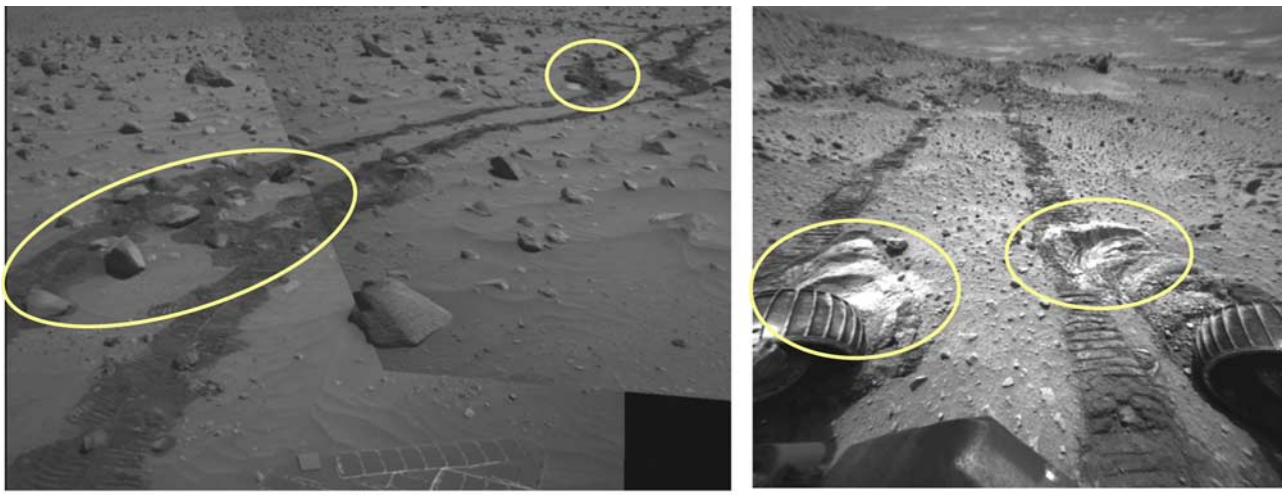

Figure 10. Examples of two anomalous traverse segments. (a) Large rocks on the track affected drive performance on segment 63 (Sol 330 to Sol 331) and (b) Rover wheels were used to excavate a trench for soil study on segment 100 (Sol 397 to Sol 398).

detailed analysis is performed to examine the segments, which, as a result, can be classified into four categories. The first category represents those influenced by incompleteness of data. Examples include segments 6 (Sol 164 to Sol 165) and 7 (Sol 165 to Sol 172). For these two segments, BA used only images taken at the beginning and end rover positions, while telemetry data include additional intermediate positions, which are relatively far from the BA straight segments and no images were taken at these middle way positions for BA. The second category contains very short segments, including segments 208 (Sol 590), 209 (Sol 590 to Sol 591), 219 (Sol 604), 238 (Sol 626) and 239 (Sol 626). The lengths of these segments are all shorter than 0.05 m. For the reason mentioned in section 5.1.2, they do not contribute significantly to the overall accumulated slippage. The third category represents places where the rover's progress was altered by large rocks on the track (Figure 10a), such as segments 63 (Sol 330 to Sol 331), 64 (Sol 331 to Sol 332), 249 (Sol 641 to Sol 642), 250 (Sol 642 to Sol 648), and 268 (Sol 670 to Sol 671). Within these segments, the obstacles caused additionally more slips. The fourth category gives special cases where special events may increase additional slips. For example, the rover excavated a trench by the rover wheels at Paso Robles in order to examine the bright soil deposit around segment 100 (Sol 397 to Sol 398, Figure 10b). Another example is that from segment 68 to segment 72 (Sol 337 to Sol 348) a rock was stuck in the right rear wheel [*Arvidson et al.*, 2006]. This makes the segments incomparable. All segments that fall in the above four anomalous traverse segment categories will be excluded for further analysis in this paper.

5.2. Analysis of Rover Slippage of Short Segments with VO Measurements

[39] Many short segments along the traverse are measured by VO, for example, for precision target approaching or for accounting for rover slips caused by difficult terrain. The segments are 0.51 m on average with 0.72 m as a maximum and 0.05 m as a minimum. VO images were taken at each step that is on average about 25 cm and rover position and attitude estimates are given per step, which provide highly accurate estimates of both rover slippage and the local terrain slope at the rover location. To effectively analyze the rover slips, only segments produced by straight drives are considered. Excluded are drives of arcs on turn-in-place. The VO estimates of pitch and roll angles at each step are used as longitudinal and lateral slopes, respectively. To account for the rover driving in both forward and backward directions, we use the absolute values of slopes and slippage [*Angelova et al.*, 2007]. In this section, the downlinked telemetry data are examined so that drives with VO performed are separated so that the nature of the slips of the short traverse segments and the effectiveness of VO can be studied. Note that in this case, the telemetry data does not include VO results.

[40] Figure 11 shows longitudinal (Figure 11a) and lateral (Figure 11b) slippages of involved steps estimated by using VO data as a function of the slopes for each individual terrain type. Considering the longitudinal slip, we can observe some distinctive slip behaviors as a function of slopes for different terrains. Slip on fine grain material is relatively large for low slopes (<5°) and increases quickly to 100% on slopes as early as 10° to 15°. Other terrain categories observed significantly less slippage for such slopes. A direct opposite in terms of slip behavior is the bedrock class which shows about 0 slip for slopes until above 25° where large slippage greater than 100% occurs. Clasts show a less stable behavior, measuring large slippage on above 10° slopes, but also allowing traverse of slopes of 20° and above. The variation within this category may contribute to less and more slippage by embedding clasts on the ground or lying loosely on top, respectively. Sand-sized materials have a similar slip behavior as the fine grain category, but generally at a lower slippage level, particularly on slopes over 10°.

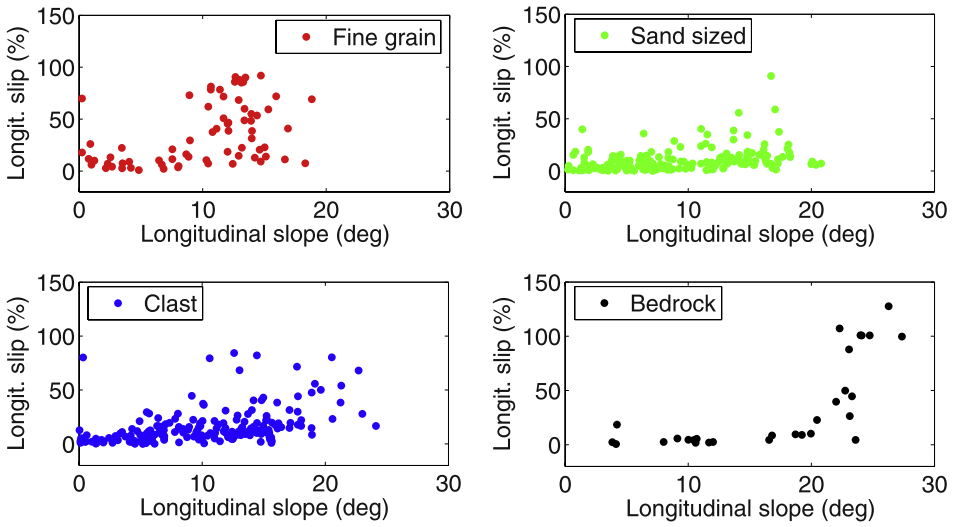

(a)

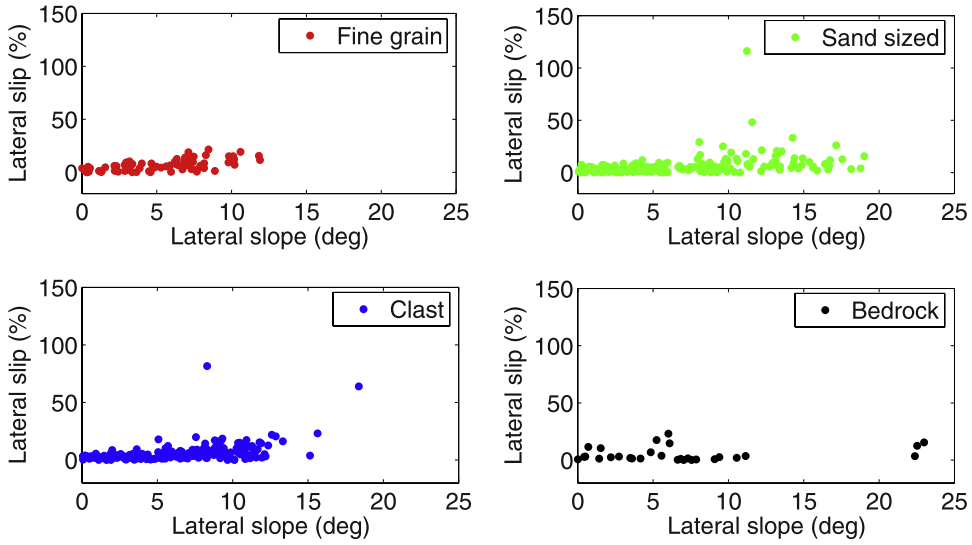

(b)

Figure 11. Slippage as a function of slope for individual terrain types estimated from VO measurements: (a) longitudinal slippage with respect to longitudinal slope and (b) lateral slippage with respect to lateral slope.

[41] For lateral slip, its functional correspondence on lateral slope is less pronounced (Figure 11b). With respect to terrain classes, again, we see comparatively larger slip values for fine grain terrain on smaller slopes than for the rest of the terrain types. A strong performance is found for the bedrock class: almost 0 lateral slip for slopes up to 22°. The other two terrains exhibit similar behavior, however, with larger slippage on higher lateral slopes around 10° and higher.

[42] Some missing values in Figure 11 can be indicative of an inability to traverse certain slope ranges on certain terrains or unavailability of data sets. For example, since 100% slip occurs on longitudinal slopes as early as 10° on fine grain terrain, it is clear that this is the maximum traversable longitudinal slope. However, it may not be concluded that lateral slopes larger than those measured in Figure 11 cannot be traversed by the rovers because such a capability also depends on the longitudinal slope at which these measurements are made. In practice, we need to consider both longitudinal and lateral slip as a function of both slopes as indicated by *Angelova et al.* [2007]. In that case, more data are needed for such an analysis.

[43] The slip analysis results of these short traverse segments can be used to characterize terrains with regard to

Table 5. Normalized Rover Slippage With Respect to Slopes

Slope	Distance Traversed (m)	Accumulated Slippage (m)	Total Normalized Slippage (%)
Upslope	1284	189	15
Downslope	1283	174	14

rover mobility, build a slip prediction model for a range of slopes and a set of terrain types [*Angelova et al.*, 2007], or determine a critical slope value for each terrain type which allows safe drive of the rover. Being able to have such estimates is crucial because unexpected rover slippage can slow down the vehicle significantly. In the worst case scenario, such knowledge can help the rovers avoid being trapped in soils of low traction [*Biesiadecki et al.*, 2006].

[44] Although the VO-based slip measurements and slopes are of the best quality we can presently obtain from onboard data, there may exist noisy measurements and/or outliers as in Figure 11. One of the error sources may come from terrain classification. Currently, we use a manual method of terrain classification for a relatively long traverse segment from rover images. More detailed and precise terrain classification along the track where slip may occur should be performed. Such information is currently not available. Other factors, which cannot be captured by the current analysis, but can contribute to slips, may include rover wheel sinkage, unstable surface, and nonhomogeneous surface materials within a segment being analyzed.

5.3. Analysis of Rover Slippage of Long Traverses with BA Measurements

[45] Traverse segments used in BA are generally longer than those in VO. Therefore, the slopes of the traverse segments are estimated and the terrain classes are characterized over a relatively long distance. Furthermore, the slopes are separated into upslopes and downslopes, as determined by the elevations of the beginning and end positions of each segment, to analyze the relationship between rover slip and ascending and descending drives. Table 5 shows the statistics of rover slippage with respect to slope types. The total upslope distance of 1284 m and downslope distance of 1283 m cover approximately the same distance, and the corresponding accumulated individual slippages are 189 m and 174 m, respectively. The total normalized individual slippages (normalized by the total length of the traverse) are 15% for upslopes and 14% for downslopes. Accordingly, 52% of the rover slippages are associated with ascending drives, and 48% with descending drives.

[46] Figure 3 provides a vertical profile of the traverse that shows that the rover started the ascending drives and ended the descending drives at Husband Hill at about the same elevation. Comparing elevations computed from BA and telemetry data, we can observe that at the end of the traverse, the elevation estimated by BA is 25 m lower than that from telemetry data over the traverse distance of 2616 m, the majority created by ascending drives.

[47] Furthermore, a study was performed on finding correlation of the slippages of these long traverse segments with terrain classes. Table 6 summarizes the statistics of rover slippage with respect to terrain classes and slopes. Among the four types of terrains, bedrock surface is stable and gives small longitudinal and lateral slippages on slopes up to 15°. Although with more significant slips, Spirit managed to drive on slopes of 15–20° of the bedrock, as well as clast and sand-sized surfaces. However, there are no drives performed on fine grain slopes over 15°. Furthermore, for longitudinal slopes of 5–10°, fine-grain terrain produced a slippage of 16.6%, which is much larger than those of other terrain classes.

[48] As demonstrated in Table 6, rover slips vary and reflect the rover's mobility with respect to various terrain types. It was expected that given a terrain type, the rover slip would increase as the terrain slope increases (relative slippage in percent in Table 6). However, this expected general trend is not clearly exhibited in Table 6. Particularly, for some terrain types, for example, clast and fine grain, the higher degrees of the longitudinal slope are associated with smaller slippages. This leads to the explanation that when

Table 6. Rover Slippage Along BA Traverse Segments With Respect to Terrain Classes and Slopes

		Longitudinal Direction				Lateral Direction			
Terrain Class	Slope Range (degree)	Segment Counts	Total Distance Traversed (m)	Total Slippage ΔS_{long} (m)	Relative Slippage (%)	Segment Counts	Total Distance Traversed (m)	Total Slippage ΔS_{lat} (m)	Relative Slippage (%)
Bedrock	0–5	0	-	-	-	3	11.02	0.34	3.1
	5–10	3	13.01	0.41	3.2	0	-	-	-
	10–15	1	8.44	0.04	0.5	0	-	-	-
	15–20	3	7.15	1.32	18.4	4	17.58	5.73	32.6
	20+	0	-	-	-	0	-	-	-
Clast	0–5	62	628.05	64.70	10.3	73	924.91	70.97	7.7
	5–10	58	617.82	55.32	8.9	59	388.97	31.35	8.1
	10–15	23	129.48	10.57	8.2	18	98.43	7.32	7.4
	15–20	7	36.96	2.29	6.2	0	-	-	-
	20+	0	-	-	-	0	-	-	-
Sand-sized	0–5	49	528.56	21.25	4.0	46	361.73	44.73	12.4
	5–10	36	239.49	23.77	9.9	36	218.91	18.40	8.4
	10–15	16	54.02	4.10	7.6	20	208.98	15.11	7.2
	15–20	4	9.52	0.85	8.9	3	21.68	0.89	4.1
	20+	1	0.02	0.004	20.0	1	20.32	0.24	1.2
Fine grain	0–5	10	164.04	6.93	4.2	10	131.19	2.36	1.8
	5–10	9	61.78	10.25	16.6	12	96.42	6.72	7.0
	10–15	4	4.33	0.27	6.3	1	2.53	0.12	4.9
	15–20	0	-	-	-	0	-	-	-
	20+	0	-	-	-	0	-	-	-

dealing with high slopes on many occasions, VO was commanded and the VO corrections are employed and included in telemetry data, which were subsequently used in BA as an input and created smaller slippages for the high slopes. We were able to trace back to some data available in the system to have a preliminary analysis. For example, in four places on the ascending route (Sol 332, Sols 337–338, Sol 366, and Sol 406) the BA-calculated slippages are all within one meter. However, the VO record indicated corrections of several meters that must be included in the telemetry data. In addition, the slope is computed using elevations at both ends of each segment and may not be representative if the terrain slope changes in the middle of a long segment. Further work on streamlining data downloading and analysis of onboard VO data, the record of VO corrections, and the BA data needs to be performed in order to give a more quantitative result. This may be done post mission when a systematic data organization and an overall BA of the traverse will be performed.

6. Summary

[49] On the basis of the available data of the MER mission we observed that the slippage of Spirit rover canceled out as the rover ascended and then descended Husband Hill, which contradicts the general trend of the rest of the Spirit traverse at the landing site that slippage accumulates along with the distance traversed. Various data and observations collected by the rover are used to analyze the contributing factors. Computational results of BA and VO are employed to quantify the slippages associated with long and short traverse segments considering different terrain types. Consequently, we can draw the following conclusions:

[50] 1. Along the Spirit traverse at Husband Hill with a traverse distance of 2616 m and an elevation difference of 83.6 m, the accumulated rover slippage reached a maximum of 83.86 m around the summit on Sol 648. However, as Spirit descended to Inner Basin on the other side, the accumulated slippage is almost canceled out at the end of the traverse (6.13 m on Sol 737).

[51] 2. Slippage of the rover is highly correlated to slope directions. Eight local regions with significant slippages and nineteen traverse segments were identified and analyzed. The general trend of the slope directions in the ascending and descending portions of the traverse proves to be the main contributor to the slippage cancellation.

[52] 3. While the horizontal slippages canceled out, the elevation difference was mostly created during the ascending process and accumulated along the way.

[53] 4. Long traverse segments, in general, created more slippages than short ones. This is reflected in both the accumulated and individual slippages.

[54] 5. Spirit performed best on the bedrock surface and managed to drive on slopes up to close to 30°. Among the four terrain types, fine grain surface is most challenging for Spirit although progress was made on slopes up to 15° and slippages of over 100% occurred for short segments.

[55] The outcomes of this research will be helpful for the ongoing MER mission and for future planetary rover missions. Further research work can be performed to incorporate the results into a traverse path planning framework in which the studied factors can be examined and the rover slippage can be minimized. The results can also be employed for precision navigation to avoid potentially dangerous regions by considering expected slippage.

[56] **Acknowledgments.** This work was partially performed at the Jet Propulsion Laboratory, California Institute of Technology, under a contract with the National Aeronautics and Space Administration. Funding of this research by the Mars Exploration Program of NASA is acknowledged.

References

Angelova, A., L. Matthies, D. Helmick, and P. Perona (2006), Slip prediction using visual information, paper presented at Robotics: Science and Systems Conference, Natl. Sci. Found., Philadelphia, Pa., 16–19 August.

Angelova, A., L. Matthies, D. Helmick, and P. Perona (2007), Learning and prediction of slip from visual information, *J. Field Robotics*, *24*(3), 205–231, doi:10.1002/rob.20179.

Arvidson, R. E., et al. (2004), Localization and physical properties experiments conducted by Opportunity at Meridiani Planum, *Science*, *306*(5702), 1730–1733.

Arvidson, R. E., et al. (2006), Overview of the Spirit Mars Exploration Rover mission to Gusev crater: Landing site to Backstay Rock in the Columbia Hills, *J. Geophys. Res.*, *111*, E02S01, doi:10.1029/2005JE002499.

Bekker, M. (1969), *Introduction to Terrain-Vehicle Systems*, 846 pp., Univ. of Michigan Press, Ann Arbor, Michigan.

Biesiadecki, J., et al. (2006), Mars Exploration Rover surface operations: Driving Opportunity at Meridiani Planum, *IEEE Robotics Autom. Mag.*, *13*(2), 63–71, doi:10.1109/MRA.2006.1638017.

Cheng, Y., M. W. Maimone, and L. H. Matthies (2006), Visual odometry on the Mars Exploration rovers: A tool to ensure accurate driving and science imaging, *IEEE Robotics Autom. Mag.*, *13*(2), 54–62, doi:10.1109/MRA.2006.1638016.

Helmick, D. M., Y. Cheng, S. Roumeliotis, D. Clouse, and L. Matthies (2004), Path following using visual odometry for a Mars rover in high-slip environments, in *2004 IEEE Aerospace Conference Proceedings*, vol. 2, pp. 772–789, Inst. of Elec. and Electron. Eng., Piscataway, N. J.

Helmick, D. M., S. Roumeliotis, Y. Cheng, D. Clouse, M. Bajracharya, and L. Matthies (2005), Slip compensation for a Mars rover, in *2005 IEEE/RSJ International Conference on Intelligent Robots and Systems: Edmonton, AB, Canada, 2–6 August*, pp. 2806–2813, Inst. of Elec. and Electron. Eng., Piscataway, N. J.

Helmick, D. M., A. Angelova, M. Livianu, and L. Matthies (2007), Terrain adaptive navigation for Mars rovers, paper presented at the 2007 IEEE Aerospace Conference, Aerospace and Electron. Syst. Soc., Big Sky, Mont., 3–10 March.

Kirk, R. L., et al. (2007), Ultrahigh resolution topographic mapping of Mars with HiRISE stereo images: Methods and first results, *Proc. Lunar Planet. Sci. Conf. 38th*, abstract 1428.

Leger, C., A. Trebi-Ollennu, J. Wright, S. Maxwell, R. Bonitz, J. Biesiadecki, F. Hartman, B. Cooper, E. Baumgartner, and M. Maimone (2005), Mars Exploration Rover surface operations: Driving Spirit at Gusev crater, in *Proceedings: The International Conference on Systems, Man and Cybernetics, Waikoloa, Hawaii, USA, October 10–12, 2005*, vol. 2, pp. 1815–1822, Inst. of Elec. and Electron. Eng., Piscataway, N. J.

Li, R., F. Ma, F. Xu, L. H. Matthies, C. F. Olson, and R. E. Arvidson (2002), Localization of Mars rovers using descent and surface-based image data, *J. Geophys. Res.*, *107*(E11), 8004, doi:10.1029/2000JE001443.

Li, R., K. Di, L. H. Matthies, R. E. Arvidson, W. M. Folkner, and B. A. Archinal (2004), Rover localization and landing site mapping technology for 2003 Mars Exploration Rover mission, *Photogramm. Eng. Remote Sens.*, *70*(1), 77–90.

Li, R., et al. (2005), Initial results of rover localization and topographic mapping for the 2003 Mars Exploration Rover mission, *Photogramm. Eng. Remote Sens.*, *71*(10), 1129–1142.

Li, R., et al. (2006), Spirit rover localization and topographic mapping at the landing site of Gusev crater, Mars, *J. Geophys. Res.*, *111*, E02S06, doi:10.1029/2005JE002483.

Li, R., et al. (2007), Opportunity rover localization and topographic mapping at the landing site of Meridiani Planum, Mars, *J. Geophys. Res.*, *112*, E02S90, doi:10.1029/2006JE002776.

Maimone, M., Y. Cheng, and L. Matthies (2007), Two years of visual odometry on the Mars Exploration rovers, *J. Field Robotics*, *24*(3), 169–186, doi:10.1002/rob.20184.

Matthies, L. H. (1989), Dynamic stereo vision, Ph.D. diss., 161 pp., Carnegie Mellon Univ., Pittsburgh, Pa.

McEwen, A. S., et al. (2007), Mars Reconnaissance Orbiter's High Resolution Imaging Science Experiment (HiRISE), *J. Geophys. Res.*, *112*, E05S02, doi:10.1029/2005JE002605.

Michaud, S., et al. (2006), Rover chassis evaluation and design optimisation using the RCET, paper presented at 9th ESA Workshop on Advanced Space Technologies for Robotics, ESTEC, Eur. Space Agency, Noordwijk, Netherlands, 28–30 November.

Moore, H., R. Hutton, R. Scott, C. Spitzer, and R. Shorthill (1977), Surface materials of the Viking landing sites, Mars, *J. Geophys. Res.*, *82*, 4497–4523, doi:10.1029/JS082i028p04497.

Moore, H., D. Bickler, J. Crisp, H. Eisen, J. Gensler, A. Haldemann, J. Matijevic, L. Reid, and F. Pavlics (1999), Soil-like deposits observed by Sojourner, the Pathfinder rover, *J. Geophys. Res.*, *104*, 8729–8746, doi:10.1029/1998JE900005.

Olson, C. F., L. H. Matthies, M. Schoppers, and M. W. Maimone (2003), Rover navigation using stereo ego-motion, *Robotics Auton. Syst.*, *43*(4), 215–229.

Perko, H. A., J. D. Nelson, and J. R. Green (2006), Mars soil mechanical properties and suitability of Mars soil simulants, *J. Aerosp. Eng.*, *19*(3), 169–176, doi:10.1061/(ASCE)0893-1321(2006)19:3(169).

Reina, G., L. Ojeda, A. Milella, and J. Borenstein (2006), Wheel slippage and sinkage detection for planetary rovers, *IEEE/ASME Trans. Mechatron.*, *11*(2), 185–195, doi:10.1109/TMECH.2006.871095.

Richter, L., R. C. Anderson, R. Li, and R. Lindemann, and the MER Science Team (2005), Inferences of strength of Martian soil deposits along MER rover traverses from evaluations of vehicle sinkages as observed in wheel tracks, paper presented at 15th International Conference of the International Society for Terrain-Vehicle Systems (ISTVS), Rent All Foundation, Hayama, Japan, 25–29 September.

Richter, L., A. Ellery, Y. Gao, S. Michaud, N. Schmitz, and S. Weiss (2006), A predictive wheel-soil interaction model for planetary rovers validated in testbeds and against MER Mars rover performance data, paper presented at 10th European Conference of the International Society for Terrain-Vehicle Systems, Budapest, Hungary, 3–6 October.

Squyres, S. W., et al. (2003), Athena Mars rover science investigation, *J. Geophys. Res.*, *108*(E12), 8062, doi:10.1029/2003JE002121.

Terzaghi, K. (1996), *Soil Mechanics in Engineering Practice*, 3rd ed., 592 pp., John Wiley, New York.

A. Angelova, Department of Computer Science, California Institute of Technology, 1200 East California Boulevard, MC 136-93, Pasadena, CA 91125, USA.

R. E. Arvidson and R. Greenberger, Department of Earth and Planetary Sciences, Washington University, 1 Brookings Drive, Box 1169, St. Louis, MO 63130, USA.

K. Di, I-C. Lee, R. Li, and B. Wu, Mapping and GIS Laboratory, CEEGS, Ohio State University, 470 Hitchcock Hall, 2070 Neil Avenue, Columbus, OH 43210, USA. (li.282@osu.edu)

M. Maimone and L. H. Matthies, Jet Propulsion Laboratory, California Institute of Technology, 4800 Oak Grove Drive, Pasadena, CA 91109, USA.

L. Richer, DLR Institute of Space Simulation, Linde Hoehe, Cologne D-51170, Germany.

M. H. Sims, NASA Ames Research Center, Moffett Field, CA 94035, USA.

S. W. Squyres and R. Sullivan, Department of Astronomy, Cornell University, 308 Space Sciences Building, Ithaca, NY 14853, USA.